Nanoscale Advances

PAPER

View Article Online
View Journal | View Issue

Cite this: *Nanoscale Adv.*, 2024, **6**, 4825

Atomically dispersed Pt_1Ir_1 pair for synergetic hydrogenation of levulinic acid to γ-valerolactone†

Boyang Liu, [a] Lin-Wei Chen [b] and Lei Wang *[a]

Received 20th May 2024
Accepted 13th July 2024

DOI: 10.1039/d4na00419a

rsc.li/nanoscale-advances

Atomically dispersed metal catalysts have attracted considerable attention in various important reactions owing to their high atom utilization and specific coordination environment. However, monometallic single sites sometimes present undesirable catalytic performance, which usually need a synergistic effect with the neighboring metal atoms, such as dimers or trimers. Different metal pairs on various solid carriers have been reported; nonetheless, huge challenges remain to precisely prepare a metal pair-site. Herein, we present a versatile strategy to synthesize an atomically dispersed Pt_1Ir_1 pair *via* strong metal–sulfur interaction over porous sulfur-doped carbons. Pt_1Ir_1 pair sites presented high activity and stability for the hydrogenation of levulinic acid to γ-valerolactone.

1 Introduction

Noble metals (Pt, Au, Ir, Rh, *etc.*) present high catalytic activities in heterogeneous catalysis and energy conversion applications owing to their specific geometric/electronic structures.[1–6] Nevertheless, the high cost of noble metals restricts their widespread applications. For supported nanoparticles, only the exposed metal atoms could directly access reactants, resulting in low metal utilization. In addition, irregular surface structures or different surface sites always afford undesired byproducts during the catalytic process.[7,8] Atomically dispersed metal catalysts supported on solid carriers are of immense interest owing to their maximum metal utilization efficiency and specific electronic/geometric structures.[9–14] Generally, the surface free energy of the particles increased sharply with a decreased particle size; thus, isolated metal atoms are prone to aggregate into particles.[15] Single metal atoms are anchored onto solid carriers by coordinating with neighbouring atoms (S, O, N, P, *etc.*) to form different coordination environments.[16–20] Homogeneous active sites and specific electronic structures endow this class of heterogeneous catalysts with the properties of homogeneous catalysts.[21] More importantly, the catalytic performance could be versatilely regulated by tuning coordination ligands.

Although single site catalysts presented distinguished performance in various important catalytic applications, the application of this type of catalyst is limited because the adsorption/activation of small molecules need the synergetic effect of neighbouring or adjacent metal atoms. For example, the splitting of H_2 molecules usually occurs on the surface of metal particles or clusters with adjacent metal atoms.[22] In addition, the optimum configuration of reaction intermediates might need more than one metal site; thus, single atom sites could not present desirable catalytic performance.[23–25] Zeng successfully prepared high-density atomically dispersed Pt on MoS_2 nanosheets.[26] For the CO_2 hydrogenation reaction, only methanol was formed on isolated Pt sites, while formic acid and methanol were detected with the help of adjacent Pt atoms, which could not only reduce the reaction barrier, but also change the reaction path. Wang successfully prepared metal dimers over mesoporous carbon nitride *via* a "precursor-preselected" wet-chemistry strategy.[27] Fe_2 dimers presented outstanding catalytic performance for the epoxidation of *trans*-stilbene to *trans*-stilbene oxide. In addition, Lu precisely synthesized $NiCu_2$ trimers over graphitic carbon nitride through the atomic layer deposition (ALD) method.[28] $NiCu_2$ trimers displayed high activity and strong stability for the hydrogenation of acetylene. The past years have seen reports on numerous metal pairs with optimum catalytic structures;[29] yet, these approaches still face practical implementation challenges, such as the expense of metal precursors employed in synthesis and the difficulty in obtaining large-scale catalysts.

In this work, we successfully prepared atomically-dispersed Pt_1Ir_1 bimetallic catalysts *via* the sulfur-fixing strategy. The strong chemical metal–S interaction could effectively prevent the agglomeration of the metal atoms. The fully dispersed Pt_1Ir_1 pair were characterized by aberration-corrected high-angle annular dark-field scanning transmission electron microscopy, X-ray photoelectron spectroscopy, and powder X-ray diffraction. The maximizing atom utilization of the atomically-dispersed Pt_1Ir_1 pairs displayed high catalytic

[a]*School of Chemistry and Chemical Engineering, Yangzhou University, Yangzhou, 225009, Jiangsu, China. E-mail: leiwang88@yzu.edu.cn*

[b]*School of Pharmacy & Institute of Pharmaceutics, Anhui University of Chinese Medicine, Hefei, 230012, China*

† Electronic supplementary information (ESI) available. See DOI: https://doi.org/10.1039/d4na00419a

performance with synergetic effect for the hydrogenation of levulinic acid to γ-valerolactone.

2 Experimental section

2.1 Synthesis of mesoporous S–C support

The S–C carrier was prepared *via* the transition metal-assisted carbonization of molecular precursor according to a previous report.[30] Typically, 2,2-bithiophene (2 g), SiO_2 sphere (~7 nm, 2 g), and $Co(NO_3)_2 \cdot 6H_2O$ (1 g) were added into 150 mL of tetrahydrofuran (THF) and stirred for 6 hours under room temperature. The THF solvent was then removed by rotary evaporation. The dried powder was ground in an agate mortar and then carbonized at 800 °C for 2 hours with a heating rate of 5 °C min^{-1} under flowing inert N_2 atmosphere. The SiO_2 template was removed by alkaline etching with 2.0 M NaOH for 3 days. Then, the Co particle was etched with 0.5 M H_2SO_4 for 6 hours at 80 °C successively. Finally, the S–C support was obtained after drying overnight at 100 °C.

2.2 Synthesis of Pt_1Ir_1/S–C catalysts

The Pt_1Ir_1/S–C catalyst was prepared *via* the conventional wet-impregnation method. Typically, 50 mg of S–C was first dispersed into 30 mL of deionized water (DI) before a certain amount of H_2PtCl_6 (0.25 mg Pt) and $IrCl_3$ (0.25 mg Ir) aqueous solution was added. After ultrasonic treatment for 30 min and stirring for 12 h, the DI was removed by rotary evaporation. The metal salts/S–C samples were reduced at 300 °C following 5% H_2/Ar for 2 h with a heating rate of 5 °C min^{-1}. The mono metallic Pt_1/S–C and Ir_1/S–C catalysts were also prepared by a similar process with 1 wt% content.

2.3 Catalysts' characterization

Transmission electron microscopy (TEM) images were obtained using a JEOL-2010F transmission electron microscope with an acceleration voltage of 120 kV. High-angle annular dark-field scanning transmission electron microscopy (HAADF-STEM) images and energy dispersive X-ray spectroscopy (EDS) mappings were conducted on an FEI Talos F200X operated at 200 kV. Aberration-corrected HAADF-STEM was performed on a JEM-ARM200F with accelerating voltage of 200 kV. Powder X-ray diffraction (XRD) analysis was conducted on a Rigaku Smartlab equipped with Cu Kα radiation ($\lambda = 1.54056$ Å) in the 2θ range of 20°–80° at a scanning speed of 10° min^{-1}. The chemical states of the bimetallic Pt_1Ir_1/S–C catalysts were analyzed by X-ray photoelectron spectroscopy (XPS) performed on a Thermo Fisher Scientific K-Alpha with an Al Kα source (1486.6 eV). The binding energy for all the elements were calibrated with the C 1s peak (284.8 eV) of adventitious carbon. The metal content was determined using an Optima 7300 DV (PerkinElmer) inductively coupled plasma atomic emission spectrometry (ICP-AES) instrument. The Pt metal was digested in aqua regia overnight at 373 K, while the digestion of Ir metal was done in a high-pressure reactor at 160 °C for 8 hours. X-ray absorption near edge structure (XANES) measurement of S L-edge was performed at the BL11U beamline of the National Synchrotron Radiation Laboratory (Hefei) operated at 0.8 GeV and 300 mA. The Brunner–Emmet–Teller (BET) surface area and pore size distribution of the support were measured by N_2 sorption isotherms (77 K) and the Barrett–Joyner–Halenda model with an Autosorb-iQ (Quantachrome Instruments, USA).

2.4 Catalysts performance evaluation

In a typical experiment, 0.5 mmol of levulinic acid, 5 mg of Pt_1Ir_1/S–C catalyst, and 2 mL of solvent were added into a glass reaction vessel. Next, the reaction vessel was first ultrasonicated for five minutes and loaded into an autoclave reactor (Parr reactor, 300 mL). The autoclave reactor was then purged with pure H_2 for five times and pressurized to 4.0 MPa. The reactor was preheated to 180 °C and then stirred at 800 rpm to eliminate external mass transfer limitations. Orthoxylene was introduced into the reaction system as an internal standard after the reaction was finished and the autoclave was submerged in freezing water. Finally, the reaction products were analyzed using a Shimadzu gas chromatograph with a flame ionization detector with high-purity nitrogen as the carrier gas. The activity was calculated under the conversion of <25% based on the total amount of metal. For the recycling test, the catalyst was separated by centrifugation, washed with ethanol and ethyl acetate successively, and then reduced at 200 °C in H_2/Ar for 2 h.

3 Results and discussion

3.1. Synthesis and characterization of the catalysts

The S–C material showed a distinct hysteresis loop, as seen by the N_2 adsorption–desorption isotherms, suggesting that the S–C material presented typical mesopores (Fig. 1a). The as-prepared mesoporous S–C carrier presented a large BET surface area of 1070 m^2 g^{-1}, and the main pore size diameter was about 7 nm (Fig. 1b), which is regulated by the SiO_2 sphere template. The sulfur content of S–C was >11.3 wt%, as revealed by elemental analysis, and no obvious particles or clusters were observed after leaching by H_2SO_4 (Fig. 1c). A small amount of Co

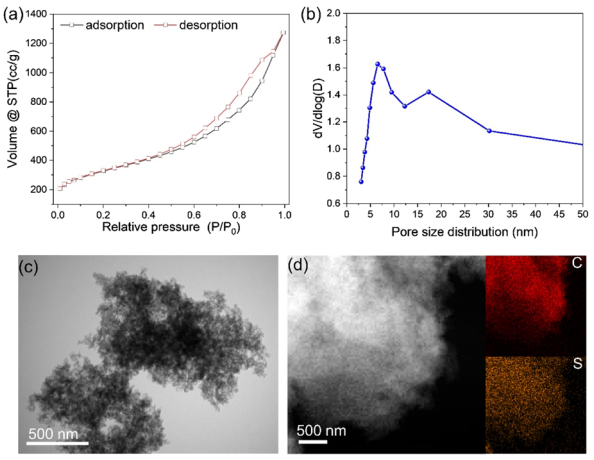

Fig. 1 (a and b) N_2 adsorption–desorption isotherms (a) and pore size distribution (b) of the S–C carrier. (c and d) TEM (c) and EDS-mappings (d) of the mesoporous S–C support.

species (~0.18 wt%) was left in the S–C carrier. EDS-mapping demonstrated the homogeneous distribution of sulfur in the mesoporous S–C support (Fig. 1d).

The Pt_1Ir_1/S–C catalysts were then synthesized *via* a traditional impregnation method that involved the wet impregnation of chloroplatinic acid and iridium chloride onto the S–C carrier and subsequent high-temperature reduction at 300 °C in H_2 atmosphere. As revealed by the TEM and HAADF-STEM images (Fig. 2a and b), no obvious metal particles or tiny clusters were observed, demonstrating the high dispersion of the PtIr/S–C catalyst. The Pt and Ir metal atoms were homogeneously dispersed over the S–C carrier according to the EDS-mapping (Fig. 2b, S1 and S2†). No specific metal XRD peak was observed in the XRD pattern for PtIr/S–C sample according to the Pt (PDF#04-0802) and Ir (PDF#06-0598) PDF card (Fig. 2c), indicating the low crystallinity and absence of large metal particles. The broad peaks at 2θ ~26° and 43° are attributed to the low graphitization degree of the S–C material.[31] Aberration-corrected HAADF-STEM was taken to further identify the fine structure of the highly dispersed PtIr/S–C (Fig. 2d). Single atoms (white circles), dimers (yellow rectangles), and cluster with 4–6 atoms (red squares) were observed. Rough statistics based on the total atoms indicated that less than 20% of isolated single atoms were distributed over the S–C support. Most metal atoms were present in the form of dimers or clusters onto the S–C carrier (denoted Pt_1Ir_1/S–C), which is illustrated in Fig. 2e. The highly dispersed metals might be ascribed to the strong metal–S coordination.[30,32,33] XPS results demonstrated that all the metal species for the atomically dispersed catalysts were in the same oxidation state (Fig. S3†), demonstrating charge transfer between the metal and S–C support *via* metal–S coordination, which is consistent with most of the reported single atom catalysts. The oxidized Pt site might provide a Lewis acid center during the synergetic hydrogenation process.[34]

As seen in Fig. 3a, two obvious new peaks at ~174 and 183 eV were detected at the S L-edge XANES for Pt_1/S–C, demonstrating that the metal–S bond was formed during the high temperature reduction process.[33] Nevertheless, no obvious metal–S bond was found for the Ir_1/S–C catalyst, indicating the relatively weak metal–sulfur interaction for the formation of the Ir_1/S–C catalyst. Liang reported that the S 2p peak in the PtCo alloy shifted to a higher binding energy (0.1 eV) compared with the S–C carrier, demonstrating the electron transfer from S atoms to metal atoms.[33] Nonetheless, we did not observe obvious changes among Pt_1Ir_1/S–C, Pt_1/S–C, Ir_1/S–C, and S–C carrier. This result might be ascribed to the low metal loading or less

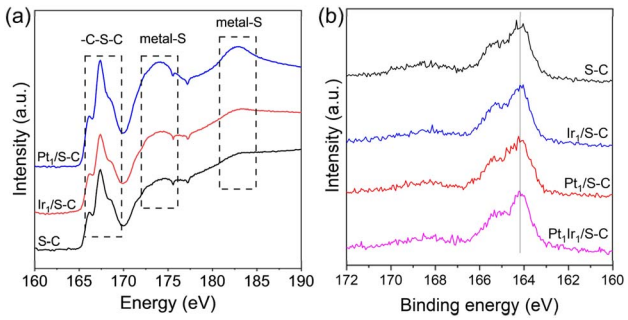

Fig. 3 Characterization of metal–sulfur interaction. (a) XANES spectra at the S L-edge of the Pt_1/S–C, Ir_1/S–C, and S–C carrier. (b) XPS spectra (S 2p) of the Pt_1Ir_1/S–C, Pt_1/S–C, Ir_1/S–C, and S–C carrier.

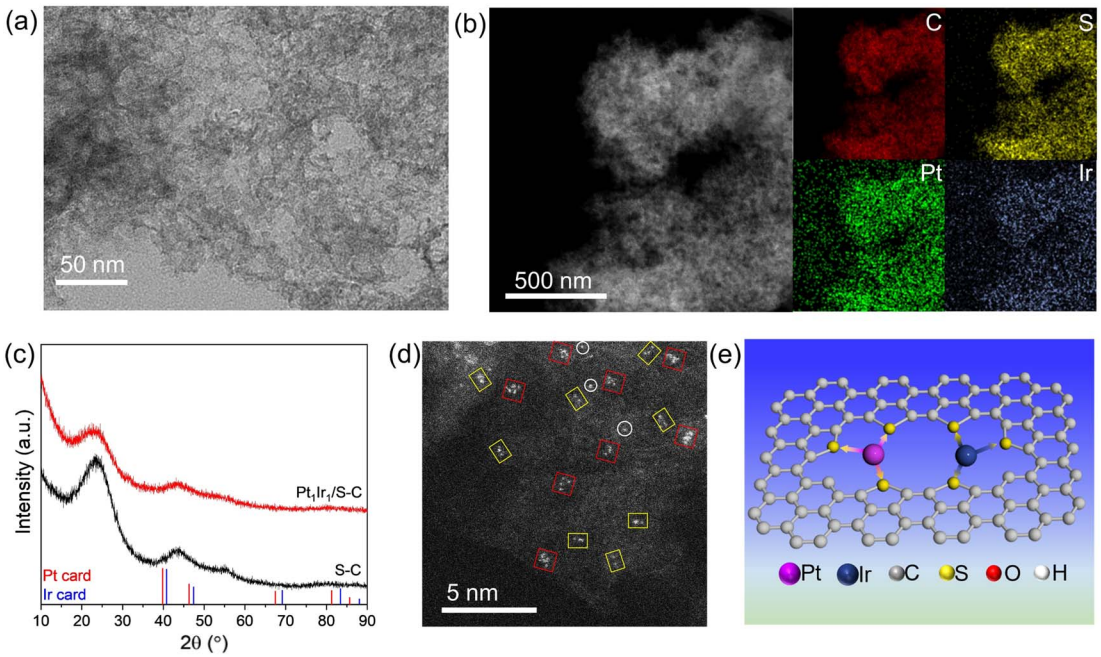

Fig. 2 Characterization of the atomically dispersed Pt_1Ir_1/S–C catalyst. TEM (a) and (b) HAADF-STEM images of Pt_1Ir_1/S–C. (c) XRD curves of S–C and PtIr/S–C. (d) Atomic-resolution HAADF-STEM image of Pt_1Ir_1/S–C, where representative isolated atoms (Pt or Ir), dimers, and clusters are highlighted by white circles, yellow rectangles, and red squares, respectively. (e) Schematic of the Pt_1Ir_1 pair over the S–C support.

electron transfer from sulfur atoms to the metal atoms under relatively low reduction temperatures. In addition, the surface sulfur atoms decreased after all the samples underwent high temperature reduction treatment (Fig. S4 and Table S1†). The metal content of Pt and Ir was determined with ICP-AES (Table S2†), which was very close to the theoretical value.

3.2 Catalytic performance for the hydrogenation of LA to GVL

The selective hydrogenation of biomass into renewable value-added products is a promising route to replace the traditional petroleum feedstock.[35] For example, γ-valerolactone (GVL) can be used as a solvent, food and fuel additive, and intermediate for fine chemicals, which can be directly obtained from the selective hydrogenation of levulinic acid (LA) with H_2 as the hydrogen donor (Scheme 1).[36,37] GVL would undergo undesirable consecutive hydrodeoxygenation reactions to form 1,4-pentanediol and methyltetrahydrofuran (Scheme 1). Thus, we selected the hydrogenation of LA to GVL under different conditions as a model reaction to investigate the utility of this class of atomically-dispersed Pt_1Ir_1 pairs.

The hydrogenation of LA was conducted in an autoclave reactor at high temperature. Monometallic Pt/S–C and Ir/S–C were also tested for comparison. The Pt/S–C and Ir/S–C in this work were atomically distributed on the S–C carrier, as we previously reported that the atomically-dispersed metal loading on S–C supports can reach up to 10 wt%. Given the importance of solvents in determining the reaction rate and product distribution, a variety of solvents has been explored in the hydrogenation of LA to GVL at 180 °C and 4 MPa H_2. The experimental results demonstrated that the activity of Pt_1Ir_1/S–C in different solvents increase in the order dioxane < *o*-xylene < H_2O < butanol (Fig. 4a). The Pt_1Ir_1/S–C catalyst presented >95% GVL selectivity in various solvents except H_2O. The catalytic performance of the single site Pt_1/S–C and Ir_1/S–C were also tested for comparation. As shown in Fig. 4c, Pt_1Ir_1/S–C presented 64% LA conversion with ~99% GVL selectivity after 4 h, while the conversion of single atom Pt_1/S–C reached only ~10% under the same reaction condition. Although the Ir_1/S–C displayed high activity, the GVL selectivity <80%, which is far greater from most of the reported results. A certain amount of 1,4-pentanediol and methyltetrahydrofuran was detected for the single atom Ir_1/S–C catalyst. To further evaluate the real activity of thePt_1Ir_1/S–C pairs, we calculated TOFs under the LA conversion below 25% for all the cases to ensure that the reaction remained under kinetic control. The Pt_1Ir_1/S–C pairs displayed a TOF value of 868 hour^{-1} for LA hydrogenation, giving about an 8-fold enhancement compared to single atom

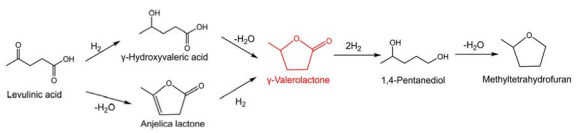

Scheme 1 Possible reaction pathways of LA hydrogenation to GVL.

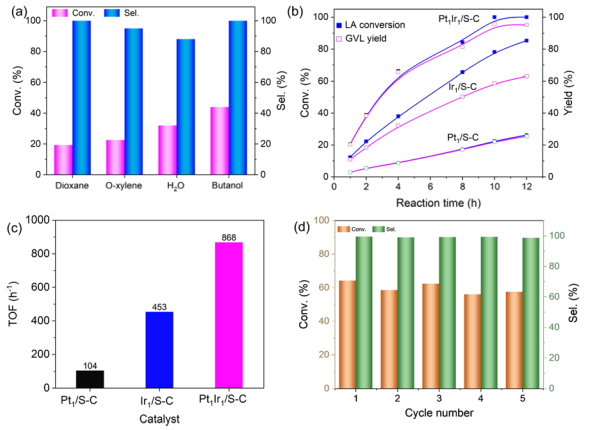

Fig. 4 Catalytic performance for the hydrogenation of LA. (a) Hydrogenation of LA over the Pt_1Ir_1/S–C catalyst in different solvents. Reaction condition: 5 mg PtIr/S–C catalyst, 1 mmol LA, 3 mL solvent, 180 °C, 4 MPa H_2, and 4 h. (b) Reaction kinetics over Pt_1Ir_1/S–C, Pt_1/S–C, and Ir_1/S–C catalysts. (c) Activity of different catalysts for the hydrogenation of LA. (d) Recycling of Pt_1Ir_1/S–C for phenylacetylene semihydrogenation within 4 h. Reaction conditions: 1 mmol LA, 3 mL butanol, 180 °C, 4 MPa H_2, and 4 h.

Pt_1/S–C catalyst (104 hour^{-1}). As demonstrated by the XANES (Fig. 3a), the low activity of the Pt_1/S–C might be ascribed to the strong chemical sulfur–Pt interaction, providing weak adsorption ability towards the reaction molecules. The high catalytic performance of Pt_1Ir_1 pairs might come from the heterolytic dissociation route for the H_2 activation process, which could robustly enhance the hydrogenation reactions. In addition, the Ir/S–C displayed much higher activity than Pt_1/S–C, demonstrating that the cleavage of H_2 is more energetically favourable on single site Ir_1/S–C than Pt_1/S–C. The hydrogenation of LA to GVL might react *via* the following mechanism. First, H_2 splits on the isolated sites with the heterolytic dissociation process at the single Ir site.[12,38] Then, the $H^{\delta+}/H^{\delta-}$ pair transfers to the carbonyl group (Fig. S5†).[39] The LA molecule is adsorbed by the hydroxyl oxygen of the carboxyl group on coordinatively oxidized Pt site (Lewis acid center).[34] Then, the Pt atom attaches two hydrogen atoms to form 4-hydroxypentanoic acid (4-HPA, intermediate). 4-HPA suffers from further dehydration process to form GVL. Then, the adjacent Pt atom might provide Lewis acid site to accelerate the reaction activity. Subsequently, the activation energy experiment was performed (Fig. S6†), in which Pt_1Ir_1/S–C and Ir_1/S–C present similar activation energy but higher than that of Pt_1/S–C, demonstrating that high temperature is more suitable for Pt_1Ir_1/S–C.

The reusability of the Pt_1Ir_1/S–C catalyst could be separated from the reaction system by filtration. After five recycling runs, the Pt_1Ir_1/S–C catalyst could nearly maintain its original activity and selectivity (Fig. 4d). No obvious agglomeration of metal atoms was observed by HAADF-STEM after recycling tests (Fig. S7†), indicating the high stability of Pt_1Ir_1 pairs on S–C when catalyzing LA hydrogenation.

4 Conclusions

In summary, we successfully synthesized atomically-dispersed Pt_1Ir_1 pairs over the sulfur-doped carbon *via* the sulfur-tethering strategy. The atomically-dispersed Pt_1Ir_1 pair presented desirable catalytic performance for the hydrogenation of LA to GVL. In contrast, the single site monometallic Pt_1 presented a very low activity. The single Ir atoms split H_2 through the heterolytic dissociation process, and the oxidized Pt synergistically accelerated the reaction activity as the Lewis acid center. The Pt_1Ir_1 pairs displayed high stability after five cycles under harsh reaction conditions. The synthesis method and synergetic effect of the atomically-dispersed metal pairs may open a new gate for fabricating dimers or trimers with an easy scale-up route for various important reactions.

Data availability

The data supporting this article have been included as part of the ESI.†

Author contributions

L. W. and B. L. contributed to the idea and experimental design and wrote the manuscript. B. L. and L.-W. C. collected data and analysed the results. All authors contributed to data analysis, interpreted the data, and approved the manuscript.

Conflicts of interest

There are no conflicts to declare.

Acknowledgements

This work is financially supported by the National Natural Science Foundation of China (22301267), Natural Science Foundation of the Jiangsu Higher Education Institutions of China (23KJD150013), and Yangzhou University Start-up Foundation.

Notes and references

1 A. H. Motagamwala, R. Almallahi, J. Wortman, V. O. Igenegbai and S. Linic, *Science*, 2021, **373**, 217.
2 H. Yan, K. He, I. A. Samek, D. Jing, M. G. Nanda, P. C. Stair and J. M. Notestein, *Science*, 2021, **371**, 1257.
3 M. Escudero-Escribano, P. Malacrida, M. H. Hansen, U. G. Vej-Hansen, A. Velázquez-Palenzuela, V. Tripkovic, J. Schiøtz, J. Rossmeisl, I. E. L. Stephens and I. Chorkendorff, *Science*, 2016, **352**, 73–76.
4 J. C. Matsubu, S. Zhang, L. DeRita, N. S. Marinkovic, J. G. Chen, G. W. Graham, X. Pan and P. Christopher, *Nat. Chem.*, 2017, **9**, 120–127.
5 S. Liu, W. Xu, Y. Niu, B. Zhang, L. Zheng, W. Liu, L. Li and J. Wang, *Nat. Commun.*, 2019, **10**, 5790.
6 L. Wang, Z. Ma, J. Xue, Z. Yuan, L.-W. Chen and S. Li, *Inorg. Chem.*, 2024, **63**, 3452–3459.
7 F. F. Tao and P. A. Crozier, *Chem. Rev.*, 2016, **116**, 3487–3539.
8 Z. Li, S. Ji, Y. Liu, X. Cao, S. Tian, Y. Chen, Z. Niu and Y. Li, *Chem. Rev.*, 2020, **120**, 623–682.
9 S. Yao, X. Zhang, W. Zhou, R. Gao, W. Xu, Y. Ye, L. Lin, X. Wen, P. Liu, B. Chen, E. Crumlin, J. Guo, Z. Zuo, W. Li, J. Xie, L. Lu, C. J. Kiely, L. Gu, C. Shi, J. A. Rodriguez and D. Ma, *Science*, 2017, **357**, 389–393.
10 Y. Zhai, D. Pierre, R. Si, W. Deng, P. Ferrin, A. U. Nilekar, G. Peng, J. A. Herron, D. C. Bell, H. Saltsburg, M. Mavrikakis and M. Flytzani-Stephanopoulos, *Science*, 2010, **329**, 1633–1636.
11 Y. Xiong, J. Dong, Z.-Q. Huang, P. Xin, W. Chen, Y. Wang, Z. Li, Z. Jin, W. Xing, Z. Zhuang, J. Ye, X. Wei, R. Cao, L. Gu, S. Sun, L. Zhuang, X. Chen, H. Yang, C. Chen, Q. Peng, C.-R. Chang, D. Wang and Y. Li, *Nat. Nanotechnol.*, 2020, **15**, 390–397.
12 P. Liu, Y. Zhao, R. Qin, S. Mo, G. Chen, L. Gu, D. M. Chevrier, P. Zhang, Q. Guo, D. Zang, B. Wu, G. Fu and N. Zheng, *Science*, 2016, **352**, 797–801.
13 S. Qian, F. Xu, Y. Fan, N. Cheng, H. Xue, Y. Yuan, R. Gautier, T. Jiang and J. Tian, *Nat. Commun.*, 2024, **15**, 2774.
14 L. Wang, S. Lyu and S. Li, *ChemPhysMater*, 2024, **3**, 24–35.
15 X.-F. Yang, A. Wang, B. Qiao, J. Li, J. Liu and T. Zhang, *Acc. Chem. Res.*, 2013, **46**, 1740–1748.
16 C. Xia, Y. Qiu, Y. Xia, P. Zhu, G. King, X. Zhang, Z. Wu, J. Y. Kim, D. A. Cullen, D. Zheng, P. Li, M. Shakouri, E. Heredia, P. Cui, H. N. Alshareef, Y. Hu and H. Wang, *Nat. Chem.*, 2021, **13**, 887–894.
17 L. Jiao, J. Li, L. L. Richard, Q. Sun, T. Stracensky, E. Liu, M. T. Sougrati, Z. Zhao, F. Yang, S. Zhong, H. Xu, S. Mukerjee, Y. Huang, D. A. Cullen, J. H. Park, M. Ferrandon, D. J. Myers, F. Jaouen and Q. Jia, *Nat. Mater.*, 2021, **20**, 1385–1391.
18 H. W. Liang, S. Bruller, R. Dong, J. Zhang, X. Feng and K. Mullen, *Nat. Commun.*, 2015, **6**, 7992.
19 C. H. Choi, M. Kim, H. C. Kwon, S. J. Cho, S. Yun, H.-T. Kim, K. J. J. Mayrhofer, H. Kim and M. Choi, *Nat. Commun.*, 2016, **7**, 10922.
20 H. Yan, H. Cheng, H. Yi, Y. Lin, T. Yao, C. Wang, J. Li, S. Wei and J. Lu, *J. Am. Chem. Soc.*, 2015, **137**, 10484–10487.
21 X. Cui, W. Li, P. Ryabchuk, K. Junge and M. Beller, *Nat. Catal.*, 2018, **1**, 385–397.
22 D. R. Aireddy and K. Ding, *ACS Catal.*, 2022, **12**, 4707–4723.
23 H. Yan, Y. Lin, H. Wu, W. Zhang, Z. Sun, H. Cheng, W. Liu, C. Wang, J. Li, X. Huang, T. Yao, J. Yang, S. Wei and J. Lu, *Nat. Commun.*, 2017, **8**, 1070.
24 Q. Wang, C. M. De Brito Mendes, O. V. Safonova, W. Baaziz, C. A. Urbina-Blanco, D. Wu, M. Marinova, O. Ersen, M. Capron, A. Y. Khodakov, M. Saeys and V. V. Ordomsky, *J. Catal.*, 2023, **426**, 336–344.
25 X. Long, J. Wang, C. Nie, Y. Xi and F. Li, *Chem Catal.*, 2024, **4**, 100810.
26 H. Li, L. Wang, Y. Dai, Z. Pu, Z. Lao, Y. Chen, M. Wang, X. Zheng, J. Zhu, W. Zhang, R. Si, C. Ma and J. Zeng, *Nat. Nanotechnol.*, 2018, **13**, 411–417.
27 S. Tian, Q. Fu, W. Chen, Q. Feng, Z. Chen, J. Zhang, W.-C. Cheong, R. Yu, L. Gu, J. Dong, J. Luo, C. Chen,

Q. Peng, C. Draxl, D. Wang and Y. Li, *Nat. Commun.*, 2018, **9**(1), 2353.

28 J. Gu, M. Jian, L. Huang, Z. Sun, A. Li, Y. Pan, J. Yang, W. Wen, W. Zhou, Y. Lin, H.-J. Wang, X. Liu, L. Wang, X. Shi, X. Huang, L. Cao, S. Chen, X. Zheng, H. Pan, J. Zhu, S. Wei, W.-X. Li and J. Lu, *Nat. Nanotechnol.*, 2021, **16**, 1141–1149.

29 E. Guan, J. Ciston, S. R. Bare, R. C. Runnebaum, A. Katz, A. Kulkarni, C. X. Kronawitter and B. C. Gates, *ACS Catal.*, 2020, **10**, 9065–9085.

30 L. Wang, M.-X. Chen, Q.-Q. Yan, S.-L. Xu, S.-Q. Chu, P. Chen, Y. Lin and H.-W. Liang, *Sci. Adv.*, 2019, **5**, eaax6322.

31 L. Wang, P. Yin, L.-L. Zhang, S.-C. Shen, S.-L. Xu, P. Chen and H.-W. Liang, *J. Catal.*, 2020, **389**, 297–304.

32 L. Z. Li, S. L. Xu, S. C. Shen, L. Wang, M. Zuo, P. Chen and H. W. Liang, *ChemNanoMat*, 2020, **6**, 969–975.

33 C.-L. Yang, L.-N. Wang, P. Yin, J. Liu, M.-X. Chen, Q.-Q. Yan, Z.-S. Wang, S.-L. Xu, S.-Q. Chu, C. Cui, H. Ju, J. Zhu, Y. Lin, J. Shui and H.-W. Liang, *Science*, 2021, **374**, 459–464.

34 I. I. Protsenko, L. Z. Nikoshvili, V. G. Matveeva and E. M. Sulman, *Top. Catal.*, 2020, **63**, 243–253.

35 Y. Gu, L. Wang, B.-Q. Xu and H. Shi, *Chin. J. Catal.*, 2023, **54**, 1–55.

36 W. Luo, M. Sankar, A. M. Beale, Q. He, C. J. Kiely, P. C. A. Bruijnincx and B. M. Weckhuysen, *Nat. Commun.*, 2015, **6**, 6540.

37 X. Gong, X. Feng, J. Cao, Y. Wang, X. Zheng, W. Yu, X. Wang and S. Shi, *Chem. Commun.*, 2023, **59**, 14717–14720.

38 A. Comas-Vives, C. González-Arellano, A. Corma, M. Iglesias, F. Sánchez and G. Ujaque, *J. Am. Chem. Soc.*, 2006, **128**, 4756–4765.

39 D. Ren, L. He, L. Yu, R.-S. Ding, Y.-M. Liu, Y. Cao, H.-Y. He and K.-N. Fan, *J. Am. Chem. Soc.*, 2012, **134**, 17592–17598.